*eng*

MDPI

*Article*

# Machine Learning Study of the Effect of Process Parameters on Tensile Strength of FFF PLA and PLA-CF

**Abdelhamid Ziadia, Mohamed Habibi * and Sousso Kelouwani**

Department of Mechanical Engineering, University of Quebec in Trois-Rivieres, 3351 Bd des Forges, Trois-Rivieres, QC G8Z 4M3, Canada; abdelhamid.ziadia@uqtr.ca (A.Z.)
* Correspondence: mohamed.habibi@uqtr.ca

**Abstract:** Material extrusion is a popular additive manufacturing technology due to its low cost, wide market availability, ability to construct complex parts, safety, and cleanliness. However, optimizing the process parameters to obtain the best possible mechanical properties has not been extensively studied. This paper aims to develop ensemble learning-based models to predict the ultimate tensile strength, Young's modulus, and the strain at break of PLA and PLA-CF 3D-printed parts, using printing temperature, printing speed, and layer thickness as process parameters. Additionally, the study investigates the impact of process parameters and material selection on the mechanical properties of the printed parts and uses genetic algorithms for multi-objective optimization according to user specifications. The results indicate that process parameters and material selection significantly influence the mechanical properties of the printed parts. The ensemble learning predictive models yielded an $R^2$ value of 91.75% for ultimate tensile strength, 94.08% for Young's modulus, and 88.54% for strain at break. The genetic algorithm successfully identified optimal parameter values for the desired mechanical properties. For optimal ultimate tensile strength, PLA-CF was used at 222.28 °C, 0.261 mm layer, 40.30 mm/s speed, yielding 41.129 MPa. For Young's modulus: 4423.63 MPa, PLA-CF, 200.01 °C, 0.388 mm layer, 40.38 mm/s. For strain at break: 2.249%, PLA, 200.34 °C, 0.390 mm layer, 45.30 mm/s. Moreover, this work is the first to model the process–structure property relationships for an additive manufacturing process and to use a multi-objective optimization approach for multiple mechanical properties, utilizing ensemble learning-based algorithms and genetic algorithms.

**Keywords:** additive manufacturing; material extrusion; machine learning; genetic algorithm; process optimization



**Citation:** Ziadia, A.; Habibi, M.; Kelouwani, S. Machine Learning Study of the Effect of Process Parameters on Tensile Strength of FFF PLA and PLA-CF. *Eng* **2023**, *4*, 2741–2763. https://doi.org/10.3390/eng4040156

Academic Editor: Tomasz Lipiński

Received: 11 October 2023
Revised: 29 October 2023
Accepted: 30 October 2023
Published: 3 November 2023



## 1. Introduction

Additive manufacturing, also known as 3D printing, is revolutionizing the manufacturing and prototyping industries by providing a simpler and more cost-effective product development process than traditional manufacturing techniques. Among various 3D printing technologies, material extrusion, or fused filament fabrication (FFF), is the most widely used and rapidly growing technique [1,2]. Material extrusion was first introduced in 1989 and patented by Scott Crump, the co-founder of Stratasys [3], who also introduced it to the market as fused deposition modeling (FDM). Initially, this technology was also referred to as fused filament fabrication (FFF), which gained popularity after the expiration of the Stratasys FDM patent [1].

The popularity of material extrusion can be attributed to its capability to print with a wide range of materials, making it possible to build new technologies with various characteristics. Additionally, its low cost, scalability, and wide market availability make it an attractive option for researchers and industry professionals alike [4].

However, research has shown that parts produced using traditional manufacturing methods exhibit superior mechanical properties compared to those fabricated with material extrusion. This is because the parts are printed layer by layer, creating voids that generate

internal stress when subjected to mechanical tests. To overcome this obstacle, researchers worldwide are pursuing different strategies to optimize the mechanical properties of 3D-printed parts by selecting the appropriate process parameters [5,6]. In summary, material extrusion has significantly improved the product development process with its versatility and cost-effectiveness. Despite its limitations in terms of mechanical properties, ongoing research aims to overcome these challenges and further enhance the capabilities of this innovative technology [4,5].

Several researchers have employed different approaches to investigate the optimization of process–structure properties of 3D-printed polymers. Gebisa et al. [5] employed a full factorial design experiment to study the effect of FFF process parameters on the tensile properties of ULTEM 9085. They investigated five variables, including the contours number, contour width, raster width, raster angle, and air gap, and found that raster angle had the greatest influence on mechanical properties. Claver et al. [6] studied the effect of layer height, infill density, and layer orientation on the tensile strength of polylactic acid (PLA) and acrylonitrile butadiene styrene (ABS). They found that infill density significantly impacted tensile strength, while layer height had little effect. Chokshi et al. [7] investigated the effect of layer thickness, infill pattern, and contours number using PLA as the printing material. Their study showed that layer thickness and contours number significantly impact flexural strength. Othman et al. [8] studied the influence of layer thickness, infill pattern, and contours number on the mechanical properties and showed that all three process parameters studied have close contribution values on mechanical strengths. Infill density has the highest influence on mechanical properties, followed by layer thickness.

To enhance the mechanical properties of polymers, researchers have developed composites that combine polymers with reinforcing materials such as fibers, particles, or fillers. Introducing these reinforcing materials allows the resulting composite material to exhibit improved properties such as increased strength, stiffness, toughness, and wear resistance compared to pure polymers. Several researchers have studied and compared the mechanical performance of polymers and composites using various materials and techniques. Ning et al. [9] evaluated the effects of carbon fibers on the mechanical properties of FFF-fabricated parts made of ABS. They found that carbon fibers enhanced tensile strength and Young's modulus but reduced toughness, yield strength, and ductility. Love et al. [10] observed that combining carbon fibers and polymers increased strength, stiffness, thermal conductivity, and reduced distortion in FFF-fabricated parts. Perez et al. [11] investigated the effects of reinforcing materials such as fibers and $TiO_2$ on the mechanical properties of 3D-printed ABS matrix composites. They found that ABS reinforced with $TiO_2$ at a 5% weight ratio showed the highest ultimate tensile strength. Aissa et al. [12] experimented with reinforced polyamide (RPA) as the printing material and used printing speed, extrusion temperature, and layer thickness as FFF process parameters. They found that extrusion temperature and layer thickness had a more significant impact on tensile strength than printing speed. Mushtaq et al. [13] used ABS as a printing material and focused on part properties like flexural strength, tensile strength, surface roughness, print time, and energy consumption. The process parameters were layer thickness, printing speed, and infill density. Using a full central composite design, twenty specimens were tested. Layer thickness was shown to be critical for achieving the optimum surface roughness and print time, while infill density was critical for mechanical qualities. Zhang et al. [14] developed a data-driven predictive modeling approach to understand the structure–property relationship of FFF-fabricated continuous carbon fiber-reinforced polymers (CCFRP). The ensemble learning algorithm combined eight base learners: multiple linear regression, least absolute shrinkage and selection operator (lasso), multivariate adaptive regression splines (MARS), generalized additive model (GAM), K-nearest neighbors (KNN), support vector machine (SVM), extra-trees, and extreme gradient boosting (XGBoost). Their study concluded that the predictive model accurately predicted the flexural strength of CCFRP specimens, with a minimum RMSE of 9.87%, a minimum RE of 7.75%, and a maximum $R^2$ of 96.99%.

The analyses of the previous investigations, summarized in Table 1, provide a presentation of an important study direction in the field of FFF, particularly with materials like PLA and PLA-CF. As previously stated, numerous researchers have conducted studies to better understand the impact of various process factors on the mechanical properties of printed parts. Several of these studies used the design of experiments, empirical methodologies, or direct experimentation to identify these relationships. Although these methodologies have produced useful insights, there appears to be a clear gap in these studies: a lack of advanced prediction and optimization strategies. While traditional methods are rigorous, they may fail to capture the complex interplay of several elements. Furthermore, it appears that the current literature lacks an integrated approach that not only predicts results but also optimizes parameters for ideal results. This identified gap emphasizes the potential need for more integrated and advanced techniques in future research initiatives.

**Table 1.** Summary of the literature review.

| Reference | Material | Parameters Studied | Major Findings |
| --- | --- | --- | --- |
| Gebisa et al. [5] | ULTEM 9085 | Contours number<br>Raster parameters<br>Air gap | Raster angle had the greatest influence on mechanical properties. |
| Claver et al. [6] | PLA, ABS | Layer height<br>Infill density<br>Layer orientation | Infill density highly impacted tensile strength; layer thickness had a smaller effect. |
| Chokshi et al. [7] | PLA | Layer thickness<br>Infill pattern<br>Contours number | Layer thickness and contours number impact flexural strength. |
| Othman et al. [8] | PLA | Layer thickness<br>Infill pattern<br>Contours number | Infill density, followed by layer thickness, have the highest influence on mechanical properties. |
| Ning et al. [9] | ABS with carbon fibers | - | Carbon fibers enhanced tensile strength and Young's modulus but reduced toughness and yield strength. |
| Love et al. [10] | Polymers with carbon fibers | - | Carbon fibers increased strength, stiffness, thermal conductivity, and reduced distortion in FDM parts. |
| Perez et al. [11] | ABS with fibers and $TiO_2$ | - | ABS reinforced with $TiO_2$ at a 5% weight ratio showed the highest ultimate tensile strength. |
| Aissa et al. [12] | RPA | Printing speed<br>Extrusion temperature<br>Layer thickness | Extrusion temperature and layer thickness influenced tensile strength more than printing speed. |
| Mushtaq et al. [13] | ABS | Layer thickness<br>Printing speed<br>Infill density | Layer thickness has a critical influence on achieving the optimum surface roughness and print time; infill density was critical for mechanical qualities. |
| Zhang et al. [14] | CCFRP | - | The predictive model accurately determined the flexural strength of CCFRP specimens. |

In this context, we present a novel way to model the process–structure properties interactions for the FFF process. The primary focus of this study is to use ensemble learning algorithms to predict the mechanical properties of FFF-printed parts using PLA and PLA with carbon fiber (PLA-CF) as the printing material. Additionally, the study aims to understand the impact of process parameters on the mechanical properties of the parts

and perform a multi-objective optimization of process parameters to achieve the desired mechanical properties. As shown in Figure 1, this novel method aims to provide a complete method that fills gaps in previous studies. The rest of this article will be organized as follows: Section 2 will define the machine learning algorithms and performance metrics used in this study. Section 3 will provide details on the experimental and computational methods adopted, and the results obtained will be discussed. Finally, in Section 4, the article will be concluded with a summary and future research perspectives.

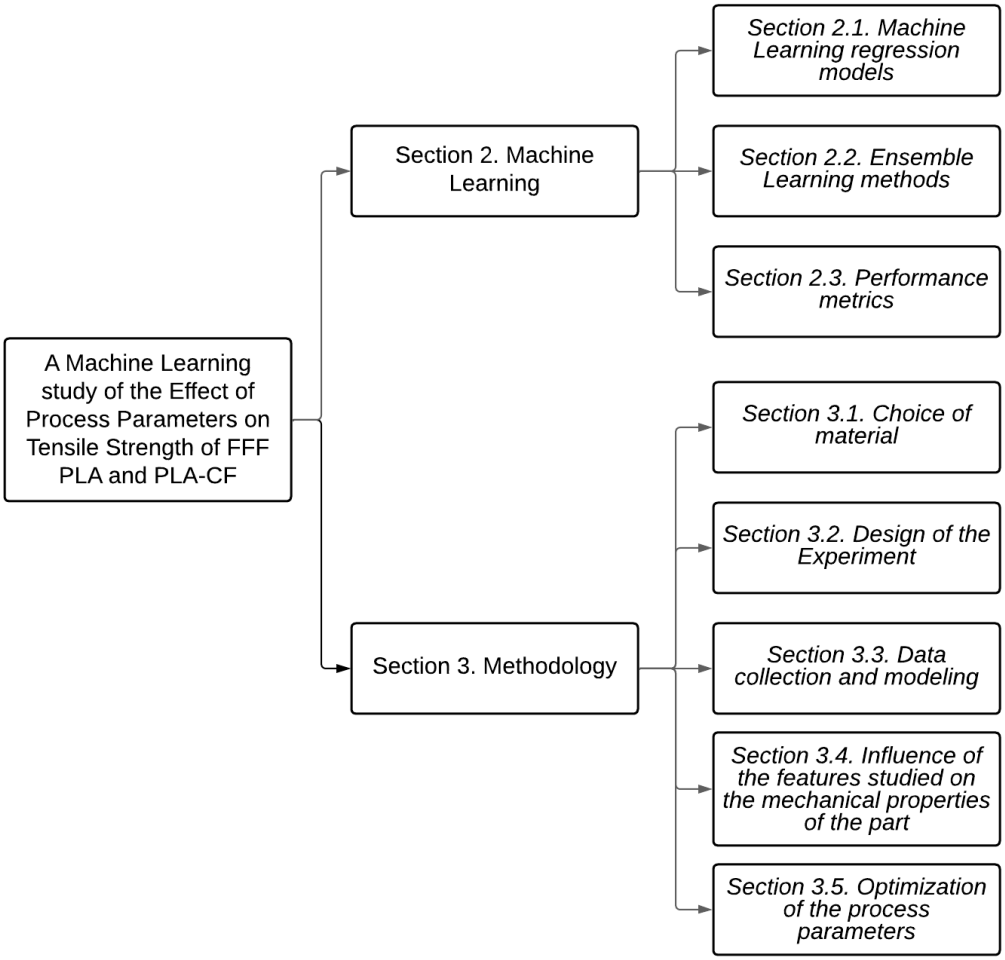


**Figure 1.** Schematic diagram of article content structure.

## 2. Machine Learning

The four main categories of machine learning techniques are supervised, unsupervised, semi-supervised, and reinforcement. However, in this paper, the focus is on supervised learning, which is a formalization of the concept of learning from examples. The supervised learning approach involves providing the learner with a training set and a test set of labeled data, which it uses to learn from the labeled data to identify the unlabeled data as accurately as possible [15]. This paper focuses explicitly on the regression-supervised models since the variables to predict are discrete.

### *2.1. Machine Learning Regression Models*

This section provides an in-depth explanation of the various machine-learning regression models employed in this study.

#### 2.1.1. Multiple Linear Regression

Multiple linear regression is a statistical method that enables the prediction of a target variable based on the values of two or more explanatory variables [16]. This technique builds upon linear regression and is sometimes referred to as multiple regression. In this context, the variable to be predicted is designated as the dependent variable, while the variables employed for prediction are called independent variables. The primary objective of this algorithm is to establish a linear association between the independent variables ($x$) and the dependent variable ($y$), as illustrated in Equation (1):

$$y = \beta_0 + \beta_1 x_1 + \cdots + \beta_p x_p \quad (1)$$

where $\beta_0$ is the value of $y$ when the independent variables are equal to zero, and $\{\beta_1, \ldots, \beta_p\}$ are the estimated regression coefficients.

#### 2.1.2. Decision Tree Regression

A decision tree is a method that employs a tree-like framework for constructing regression models [17,18]. This approach progressively develops a corresponding decision tree by dividing a dataset into increasingly smaller subsets. The decision tree consists of three types of nodes. The root node serves as the starting point and represents the entire data sample. Interior nodes symbolize the features of the dataset, with their branches denoting the respective decisions. Lastly, leaf nodes signify the outcomes derived from the model.

#### 2.1.3. Least Absolute Shrinkage and Selection Operator (Lasso)

Lasso, a shrinkage method, applies constraints on the coefficients of the least squares estimates [14]. The objective function for the lasso technique is illustrated in Equation (2):

$$J = \sum_{i=1}^{N} \left( y_i - \beta_0 - \sum_{j=1}^{p} \beta_j x_{ij} \right)^2 + \lambda \sum_{j=1}^{p} \beta_j \quad (2)$$

where $\beta_0$ and $\beta_j$ represent the coefficients for the least squares estimates, and $\lambda$ denotes the tuning parameter that regulates the penalty effect on the estimation of coefficients. The lasso offers an advantage over traditional least squares approaches as the penalty term facilitates managing the trade-off between variance and bias.

#### 2.1.4. Ridge Regression

Ridge regression, a linear regression variation, contains a regularization method to avoid overfitting and deal with multicollinearity among predictor variables. It predicts the dependent variable $y$ based on the independent variables $x_1$, $x_2$, $x_3$, …, $x_p$ via the linear relationship:

$$y = \beta_0 + \beta_1 x_1 + \beta_2 x_2 + \ldots + \beta_p x_p + \lambda \sum_{i=1}^{p} \beta_i^2 \quad (3)$$

where $\beta_0$, $\beta_1$, $\beta_2 \ldots, \beta_p$ are the coefficients estimated to minimize the residual sum of squares plus the penalty term. The presence of the penalty term $\lambda \sum_{i=1}^{p} \beta_i^2$ distinguishes ridge regression from ordinary linear regression; it penalizes large coefficients with a tuning parameter $\lambda$.

Ridge regression behaves exactly like normal linear regression when ($\lambda = 0$). As $\lambda$ increases, the model's coefficients approach zero, simplifying the model. To assist the model in predicting new data, the best value for $\lambda$ is commonly chosen through cross-validation. Ridge regression performs better when the predictors are correlated, leading to more stable predictions and preventing calculation issues.

### *2.2. Ensemble Learning Methods*

Ensemble learning is a technique that combines multiple base learners to enhance the final prediction [18]. Individual base models might exhibit suboptimal performance

due to high variance or bias. However, when these base learners are connected, they form a more robust learner, as their combination effectively reduces bias or variance, leading to improved model performance. In this study, four distinct types of ensemble learning techniques were employed.

#### 2.2.1. Bagging and Boosting

The key distinction between bagging and boosting lies in their training methodologies. In bagging, the base models are trained concurrently, whereas boosting necessitates sequential training of the base models [19].

The underlying principle of bagging ensemble learning is straightforward; it depends on samples generated using the bootstrap statistical method, which is based on an original dataset [18]. Given N bootstrap samples, each with a size of S (as shown in Equation (4)), bagging proceeds accordingly:

$$\left\{\left(r_1^1, r_2^1, \ldots, r_S^1\right), \left(r_1^2, r_2^2, \ldots, r_S^2\right), \ldots, \left(r_1^N, r_2^N, \ldots, r_S^N\right)\right\} \tag{4}$$

These samples are subsequently utilized to train multiple base models, as demonstrated in Equation (5):

$$\{m_1, m_2, \ldots, m_N\}. \tag{5}$$

In a regression scenario, as is the case in this study, the average of the predictions from the base models is computed to generate a final prediction with reduced variance, as depicted in Equation (6):

$$fm_i(x) = \frac{1}{N}\sum_{i=1}^{N} m_i(x)\,. \tag{6}$$

In this study, the bagging method employed is random forest (RF), which utilizes deep decision trees as weak learners fitted to bootstrap samples derived from an initial dataset [20]. In RF, feature sampling also occurs, ensuring that each decision tree trains on a random subset of features. Boosting shares similarities with bagging, as both techniques use multiple base models to achieve a better-performing model [18].

The primary difference between the two is that boosting trains base models sequentially, with each model focusing on the data poorly addressed by its predecessor. Upon completing the process, a learner with reduced bias is obtained. The boosting methods utilized in this study include gradient boosting and extreme gradient boosting (XGB).

Gradient boosting is an approach wherein the ensemble model is constructed as the sum of weighted weak learners, as illustrated in Equation (7):

$$fm_N(.) = \sum_{i=1}^{N} c_i \times m_i(.) \tag{7}$$

This algorithm transforms the problem into a gradient descent-based one. During each sequential iteration, a weak learner is fitted to the negative of the current fitting error in relation to the existing ensemble model [19], as demonstrated in Equation (8):

$$fm_i(.) = fm_{i-1}(.) - c_i \times \nabla_{fm_{i-1}} L(fm_{i-1})(.) \tag{8}$$

where $L(.)$ represents the fitting error of the model, $c_i$ is the step size, and $-\nabla_{fm_{i-1}} L(fm_{i-1})(.)$ denotes the opposite of the current fitting error relative to the existing model.

Extreme gradient boosting (XGB) is constructed similarly as a sum of weighted weak learners (refer to Equation (7)), where the first weak learner is trained on the entire input data. Subsequent models are trained on the residuals to address the limitations of the previous training, continuing until the stopping criterion is achieved [21].

XGB strives to prevent overfitting while optimizing computational resources [22,23]. To accomplish this, an objective function (shown in Equation (9)) that assesses both loss and regularization should be minimized:

$$Obj^{(t)} = \sum_{k=1}^{n} l(y_i, \hat{y}_i) + \sum_{k=1}^{t} \Omega(f_i). \quad (9)$$

In this case, $n$ is the number of values, $l$ denotes the loss function, $y_i$ and $\hat{y}_i$ are the actual label and the predicted label, respectively, $f_i$ is the weak learner, and $\Omega$ is the regulation term (Equation (10)), which is defined as:

$$\Omega(f_i) \equiv \gamma T + \frac{1}{2}\lambda \| w \|^2 \quad (10)$$

where $\gamma$ represents the minimum loss necessary to further partition the leaf node, $T$ denotes the number of leaves in the tree, $\lambda$ is the regularization parameter, and $w$ refers to the weight assigned to each leaf.

#### 2.2.2. Stacking

Unlike bagging and boosting methods, which rely on basic models utilizing the same algorithm, stacking models employ a hierarchical ensemble framework. The stacking model enhances modeling accuracy by combining different classifiers or regressors [24–26]. The simplest stacking model typically comprises two levels: level 0, which includes basic models, and level 1, which features the meta-learner. The basic models (level-0) utilize various algorithms to learn from the original dataset, generating the meta-feature dataset, while the meta-learner (level-1) processes the meta-feature dataset to produce the final results. K-fold cross-validation is commonly employed during the training process of a single basic model to prevent overfitting and ensure that all original datasets contribute to training for generating new meta-feature datasets.

#### 2.2.3. Blending

The primary distinction between blending and stacking lies in the manner in which basic models generate the meta-feature dataset. Instead of using the K-fold cross-validation method, blending reserves a portion of the training dataset (typically 10% or 20%) as the validation set [26]. Figure 2 provides a summary of the ensemble learning blending method.

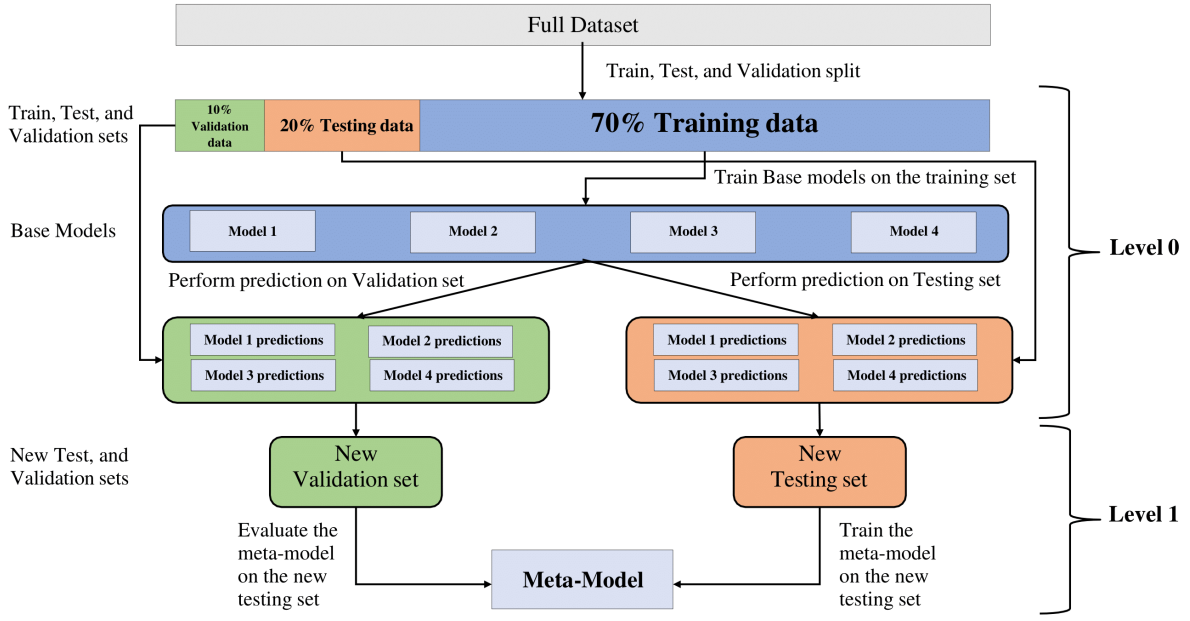


**Figure 2.** Blending method.

### 2.3. Performance Metrics

A critical aspect of developing a robust machine learning model is assessing its performance. Various metrics are employed to evaluate the quality of the model. These performance indicators facilitate the measurement of the model's effectiveness based on the available data. By fine-tuning the hyperparameters, it is possible to improve the model's performance.

#### 2.3.1. Root Mean Squared Error (RMSE)

Root mean square error (RMSE) represents the standard deviation of the prediction errors, indicating how closely the data is clustered around the best-fit line [27,28]. The formula to calculate the RMSE is shown in Equation (11):

$$\mathrm{RMSE} = \sqrt{\frac{1}{n}\sum_{i=1}^{n}(y_i - \hat{y}_i)^2} \quad (11)$$

In this equation, $y$ represents the actual value, $\hat{y}$ is the predicted value, $n$ denotes the number of values, and $i$ refers to the index of each value.

#### 2.3.2. Coefficient of Determination ($R^2$)

$R^2$, also known as the coefficient of determination, represents the difference between 1 and the ratio of the sum of residual squares to the total sum of squares [28], as shown in Equation (12):

$$R^2 = 1 - \frac{\sum_{i=1}^{n}(y_i - \hat{y}_i)^2}{\sum_{i=1}^{n}(y_i - \bar{y})^2} \quad (12)$$

In this equation, $y$ denotes the actual value, $\hat{y}$ is the predicted value, $\bar{y}$ represents the mean value, $n$ refers to the number of values, and $i$ indicates the index of each value.

An $R^2$ score of 1.0 signifies a perfect fit of the model to the data, while an $R^2$ value of 0.0 suggests that the predicted values are constant and equal to the mean value of the training data. A negative $R^2$ score implies that the model's performance is exceptionally poor.

## 3. Methodology

The CAD models of the test specimens are designed using SolidWorks and saved as STL files. These files are then processed using Ultimaker Cura 5.1.0 software, which slices the STL files and generates the G-code for printing the models with the material extrusion printer, Ultimaker S5. The test specimens are prepared for tensile strength testing in accordance with the ASTM D638-14 Type I [29] standard method. This test method aims to determine the tensile properties of unreinforced and reinforced plastics in the form of standard dumbbell-shaped test specimens when tested under specified conditions. The test specimens have an overall width of 19 mm and an overall length of 165 mm (Figure 3).

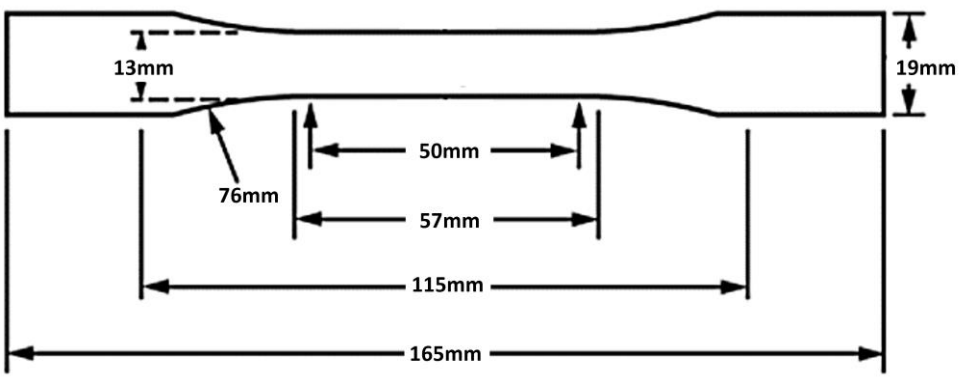


**Figure 3.** Tensile specimen shape and dimensions.

### *3.1. Choice of Material*

PLA, or polylactic acid, is a biodegradable and bioactive polyester that is derived from renewable resources, such as cornstarch, sugarcane, or cassava roots. It has become a popular material for 3D printing due to its environmental friendliness, ease of printing, and low toxicity. However, its mechanical properties are not as strong as some other materials, such as ABS.

To improve the properties of PLA, researchers have turned to composite materials, such as PLA-CF. Carbon fiber is a strong and lightweight material that can be used to reinforce plastic materials. PLA-CF is a composite material made by adding carbon fiber to PLA. It has improved mechanical properties, such as strength and stiffness, compared to pure PLA.

The use of bioplastics, such as PLA, is becoming increasingly important as concerns about the environment and sustainability grow. Petroleum-based plastics, such as ABS, are non-renewable and contribute to pollution and waste. The availability of these materials is also decreasing, making it necessary to find alternative materials that are more sustainable. By using PLA and PLA-CF, this study contributes to the development of more environmentally friendly 3D-printing materials.

### *3.2. Design of the Experiment*

The optimization of the process–structure properties of materials is a crucial aspect of 3D printing. This study considered three key parameters for optimizing the 3D printing process of PLA and PLA-CF: printing temperature, layer thickness, and printing speed.

Printing temperature refers to the temperature at which the material is extruded from the printer nozzle. It is a critical parameter that can significantly impact the final mechanical properties of the printed part. If the temperature is too low, the material may not bond well between layers, leading to a weak and brittle part. On the other hand, if the temperature is too high, the material may burn or degrade, affecting its structural integrity [30]. Layer thickness refers to the thickness of each layer of material that is deposited on top of the previous layer. This parameter affects the resolution and quality of the final printed part. A thinner layer thickness results in higher resolution and smoother surface finish, but it also increases printing time. A thicker layer thickness results in faster printing but may compromise the quality and mechanical properties of the final part [31]. Printing speed refers to the speed at which the printer moves the nozzle across the printing bed. This parameter affects the overall printing time and the quality of the final part. A slower printing speed allows for better adhesion between layers, resulting in a stronger part with a better surface finish; however, it also increases printing time. A faster printing speed reduces the printing time but may result in weaker parts with a lower-quality surface finish [32].

Other parameters, such as the infill density and pattern, and bed temperature, can also affect the final properties of the printed part. However, for this study, these parameters were set as indicated in Table 2 and were not considered in the optimization process.

**Table 2.** Table of the fixed FFF process parameters and their description.

| Factors | Description | Value |
|---|---|---|
| Bed temperature (°C) | Used to heat the build platform | 60 |
| Infill density % | The amount of material used in the inside of the print | 100 |
| Infill pattern | The form or structure of the material within the component | Lines |
| Number of contours | The number of contours surrounding the part | 1 |

The full factorial design of the experiment involves testing all possible combinations of the chosen parameter levels to determine their effect on the final properties of the printed part. As depicted in Table 3, three levels were selected for each parameter: printing temperature, layer thickness, and printing speed.

**Table 3.** Table of the selected factors and their levels.

| Factors | Level 1 | Level 2 | Level 3 |
|---|---|---|---|
| Printing temperature (°C) | 200 | 215 | 230 |
| Layer thickness (mm) | 0.25 | 0.35 | 0.45 |
| Printing speed (mm/s) | 40 | 50 | 60 |

For printing temperature, the levels chosen were 200, 215, and 230 °C. These temperatures were selected based on the melting point of the PLA and PLA-CF materials and their recommended printing temperature range.

For layer thickness, the levels chosen were 0.25, 0.35, and 0.45 mm. This parameter affects the resolution and quality of the final printed part, as well as printing time.

Finally, for printing speed, the levels chosen were 40, 50, and 60 mm/s. This parameter affects printing time and the overall quality of the printed part, as well as its mechanical properties.

By applying a full factorial design of the experiment, this study can determine the effect of each parameter and their interactions on the final properties of the printed parts. This approach allows for the optimization of the printing process and the production of high-quality parts with the desired mechanical properties.

The full factorial design of the experiment yielded 27 specimens for each material, resulting in a total of 54 specimens for the study. Of these, 27 specimens were printed using pure PLA, and the remaining 27 specimens were printed using PLA-CF. Each specimen represents a unique combination of the chosen parameter levels, allowing for the determination of how each parameter affects the final mechanical properties of the printed part. By testing multiple specimens for each material and parameter combination, the study can determine the consistency and repeatability of the printing process and ensure that the results are statistically significant.

Overall, the use of a full factorial design of the experiment and multiple specimens allows for a comprehensive analysis of the 3D printing process and the properties of the printed parts. This approach can help to optimize the printing process, improve the quality of the final parts, and contribute to the development of more sustainable and environmentally friendly 3D-printing materials.

### *3.3. Data Collection and Modeling*

Tensile tests are a standard method for determining the mechanical properties of materials, including their strength, stiffness, and ductility. In this study, the specimens created using the full factorial design of the experiment were used for tensile tests to evaluate the mechanical properties of PLA and PLA-CF.

The tensile tests were performed using a universal tensile material testing system MTS, which is a commonly used equipment for material testing. The crosshead speed was set to 2 mm/min, which is a typical speed for tensile tests on 3D-printed parts. The experimental setup for the tensile test includes the MTS equipment, the specimen holder, and the strain gauge for measuring the deformation of the specimen. After the tensile tests were performed, the obtained data were manually preprocessed and stored in CSV files. Preprocessing involves removing any outliers or errors in the data and ensuring that the data is formatted correctly for analysis. The results of data collection and preprocessing are shown in Table A1, which includes the tensile strength, modulus of elasticity, and elongation at break for each specimen.

The tensile test results are used to evaluate the effect of the chosen parameters on the mechanical properties of the printed parts. By analyzing the data and comparing the results for different parameter combinations, the optimal printing parameters can be determined for producing parts with the desired mechanical properties.

In this study, the collected data from tensile tests were used to train ensemble learning models to predict the ultimate tensile strength, Young's modulus, and strain at the break

of the printed parts. The blending ensemble learning method was used, which combines multiple weak learners to create a stronger, more accurate predictive model.

The weak learners employed were the bagging method random forest, the boosting methods Xgboost and gradient boosting, and the regression models decision tree regressor, the multiple linear regression, lasso, and ridge regression. The multiple linear regression was used as the meta-learner, which combines the predictions of the weak learners to create the final prediction.

To train and evaluate the ensemble learning models, the data was randomly split into training data (70%), testing data (20%), and validation data (10%). The weak learners were trained using the training data, and their predictions were combined to create the data on which the meta-learner was trained. The prediction results of the validation set of the weak learners were combined with the validation set to evaluate the model.

The results of the ensemble learning models (Table 4) showed a high accuracy in predicting the mechanical properties of the printed parts. The $R^2$ score for the prediction of ultimate tensile strength was 91.75%, the $R^2$ score for Young's modulus was 94.08%, and the $R^2$ score for strain at break was 88.54% (Figure 4). The RMSE values were also relatively low, indicating that the models have a good predictive accuracy.

**Table 4.** Prediction accuracy of the blending methods.

| Property Predicted | $R^2$ (%) | RMSE | Mean of Actual Values |
|---|---|---|---|
| Ultimate tensile strength (σ) (MPa) | 91.75% | 1.23 | 33.87 |
| Young's modulus (E) (MPa) | 94.08% | 278.00 | 3233.74 |
| Strain at break (ε) (%) | 88.54% | 0.09 | 1.91 |



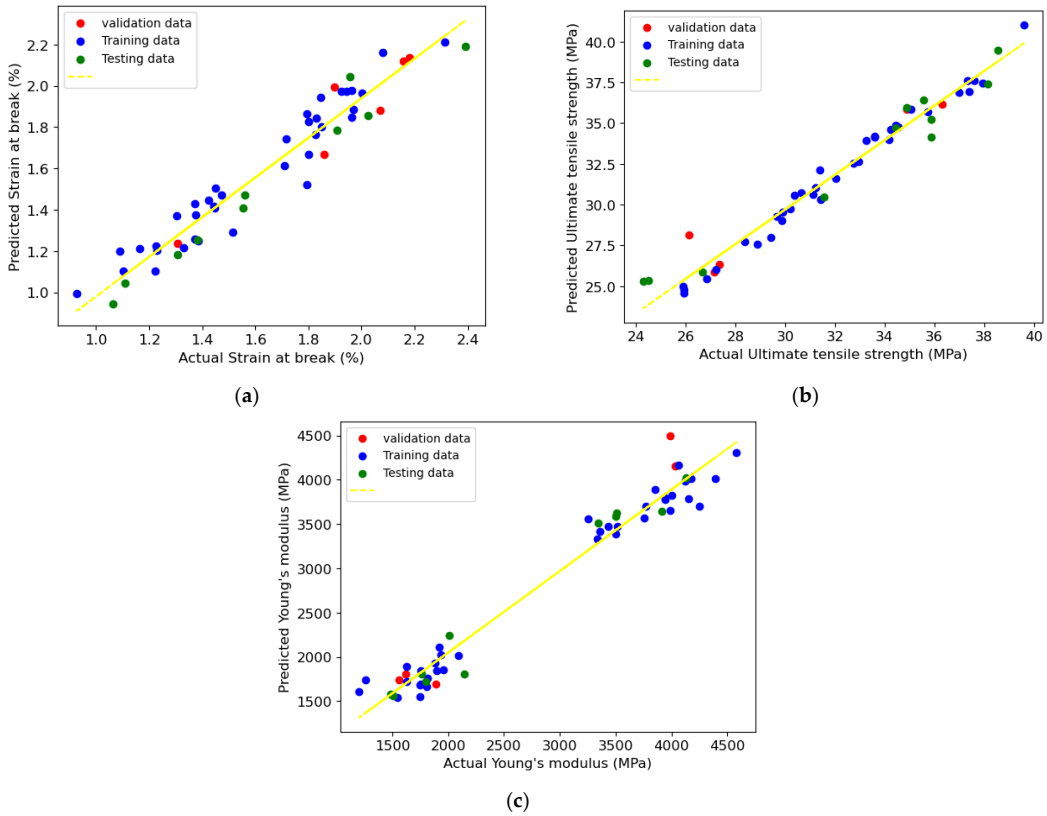


**Figure 4.** Observed versus predicted mechanical properties: (**a**) strain at break (%), (**b**) ultimate tensile strength (MPa), and (**c**) Young's modulus (MPa).

### *3.4. Influence of the Features Studied on the Mechanical Properties of the Part*

Table A1 provides data on the mechanical properties of the PLA and PLA-CF specimens. There is a clear difference between the properties of the two materials, which confirms the effect of carbon fiber on PLA. The addition of carbon fiber improves the mechanical properties of PLA, including its strength, stiffness, and toughness.

Figure 5 presents the behavior of runs 1, 10, 12, and 13 of PLA and PLA-CF. These runs represent different combinations of the printing parameters and their effect on the mechanical properties of the printed parts. The plots show the stress–strain curves for

These results prove that the models trained can predict the mechanical properties studied with high accuracy. Therefore, the optimization of the process parameters within the range studied became possible. Consequently, it is necessary to analyze the influence of the process parameters used on these mechanical properties.

### *3.4. Influence of the Features Studied on the Mechanical Properties of the Part*

Table A1 provides data on the mechanical properties of the PLA and PLA-CF specimens. There is a clear difference between the properties of the two materials, which confirms the effect of carbon fiber on PLA. The addition of carbon fiber improves the mechanical properties of PLA, including its strength, stiffness, and toughness.

Figure 5 presents the behavior of runs 1, 10, 12, and 13 of PLA and PLA-CF. These runs represent different combinations of the printing parameters and their effect on the mechanical properties of the printed parts. The plots show the stress–strain curves for each run, which provide information on the mechanical behavior of the printed parts under a tensile load.



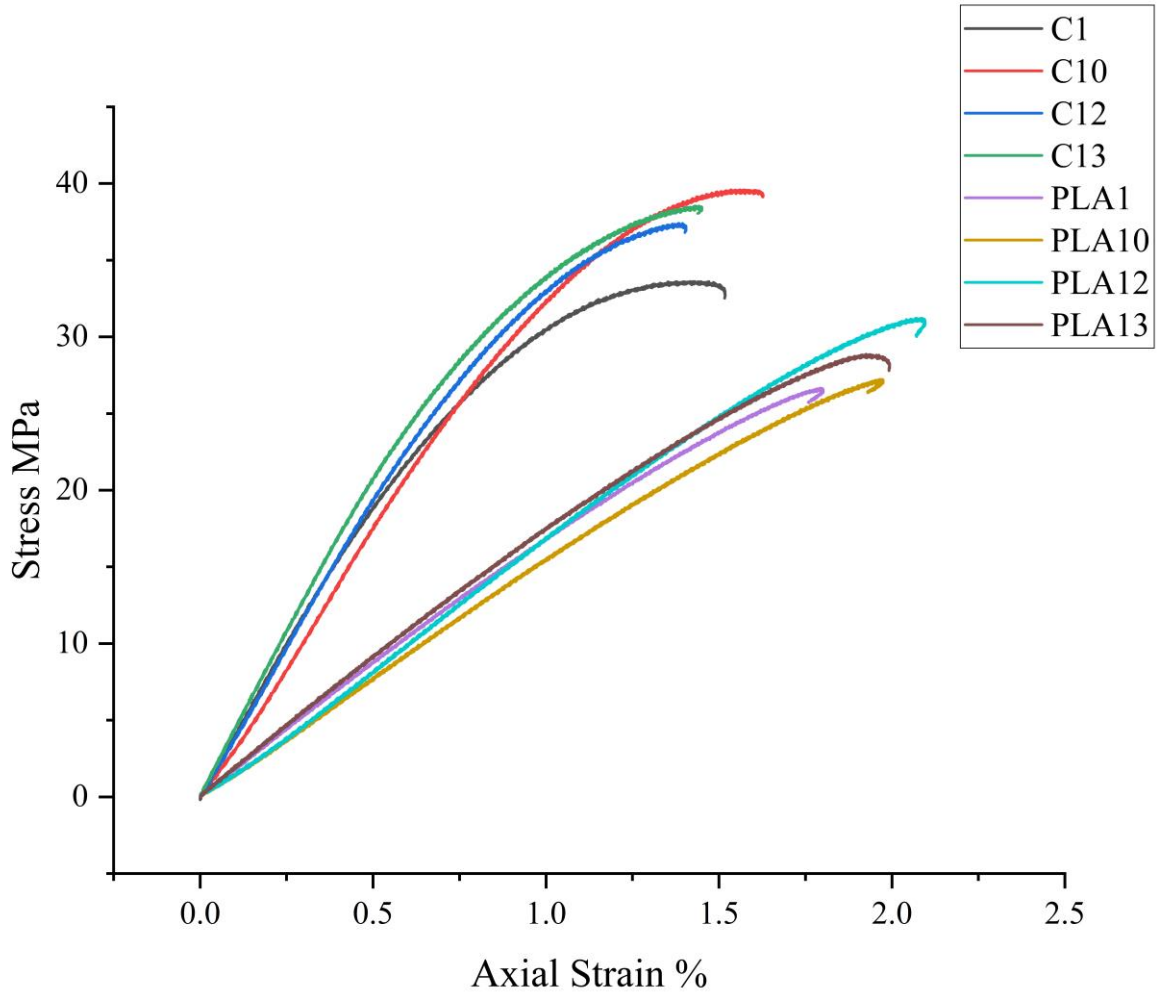


**Figure 5.** Tensile test behavior of PLA and PLA-CF parts.

**Figure 5.** Tensile test behavior of PLA and PLA-CF parts.

#### 3.4.1. Feature Importance

The decision tree regressor algorithm was used to study the importance of the features, as it provides good interpretability and the ability to output the importance of the features. The importance of the features indicates the extent to which a given input feature affects the outcome, which can be used to evaluate the relative influence of the input features on the mechanical properties of the printed parts.

3.4.1. Feature Importance

The decision tree regressor algorithm was used to study the importance of the features, as it provides good interpretability and the ability to output the importance of the features. The importance of the features indicates the extent to which a given input feature affects the outcome, which can be used to evaluate the relative influence of the input features on the mechanical properties of the printed parts.

The results presented in Table 5 show that the material had the greatest importance on all the mechanical properties studied, which confirms the significant effect of carbon fiber on the mechanical properties of PLA, which is supported by various studies. In fact,

The results presented in Table 5 show that the material had the greatest importance on all the mechanical properties studied, which confirms the significant effect of carbon fiber on the mechanical properties of PLA, which is supported by various studies. In fact, Ning et al. [9] deduced that the inclusion of carbon fibers into ABS significantly increased its tensile strength and Young's modulus, albeit with a noted reduction in toughness, yield strength, and ductility, which is consistent with our observations regarding the significant improvement in mechanical performance through the use of carbon fiber reinforcement. Similarly, Love et al. [10] confirmed that combining carbon fibers with polymers increased strength, stiffness, and heat conductivity while decreasing distortion in FFF-fabricated parts.

**Table 5.** Features importance for each mechanical property studied using a decision tree.

| | Ultimate Tensile Strength | Young's Modulus | Strain at Break |
|---|---|---|---|
| Material (PLA/PLA-CF) | 67.30% | 92.70% | 71.60% |
| Printing temperature | 12.89% | 2.44% | 7.08% |
| Layer thickness | 9.68% | 2.99% | 13.19% |
| Printing speed | 10.11% | 1.85% | 8.12% |

The study of feature importance also confirms that the printing temperature has the most significant influence on the ultimate tensile strength of the printed parts. For Young's modulus and strain at break, the layer thickness was the process parameter with the most significant influence, as shown in Figure 6, which showcases the influence of the process parameters on the mechanical properties of the printed parts. In a study conducted by Aissa et al. [12], printing temperature had a greater influence on tensile strength than other FFF process factors, such as layer thickness and printing speed. Furthermore, other researchers' investigations of various process–structure properties of FFF-printed polymers, as noted in Gebisa et al. [5] and Claver et al. [6], demonstrated the importance of optimal process parameter settings, with printing temperature emerging as a critical determinant of mechanical properties. These findings highlight the major influence of printing temperature on the mechanical properties of FFF-printed objects. The results of feature importance also revealed the critical function of layer thickness in affecting mechanical properties. This discovery is supported by Othman et al. [8], who emphasized the significance of layer thickness in their work, citing its strong association to mechanical strengths when paired with other parameters. Aissa et al. [12] discovered layer thickness as a key FFF process parameter impacting tensile strength, stressing its importance in 3D printing. They also stated that printing speed has a smaller impact on mechanical properties compared to layer thickness and printing temperature.

*Eng* **2023**, *4*, FOR PEER REVIEW 14

parameters on the mechanical properties of the printed parts. In a study conducted by Aissa et al. [12], printing temperature had a greater influence on tensile strength than other FFF process factors, such as layer thickness and printing speed. Furthermore, other researchers' investigations of various process–structure properties of FFF-printed polymers, as noted in Gebisa et al. [5] and Claver et al. [6], demonstrated the importance of optimal process parameter settings, with printing temperature emerging as a critical determinant of mechanical properties. These findings highlight the major influence of printing temperature on the mechanical properties of FFF-printed objects. The results of feature importance also revealed the critical function of layer thickness in affecting mechanical properties. This discovery is supported by Othman et al. [8], who emphasized the significance of layer thickness in their work, citing its strong association to mechanical strengths when paired with other parameters. Aissa et al. [12] discovered layer thickness as a key FFF process parameter impacting tensile strength, stressing its importance in 3D printing. They also stated that printing speed has a smaller impact on mechanical properties compared to layer thickness and printing temperature.

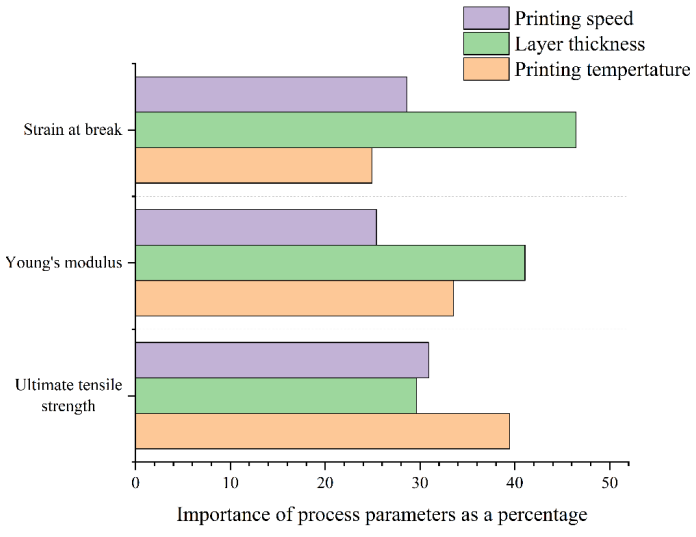


**Figure 6.** Importance of the process parameters on the mechanical properties.

**Figure 6.** Importance of the process parameters on the mechanical properties.

**Table 5.** Features importance for each mechanical property studied using a decision tree.

| | Ultimate Tensile Strength | Young's Modulus | Strain at Break |
|---|---|---|---|

These findings can be used to optimize the printing process and improve the mechanical properties of the printed parts. By selecting the appropriate material and optimizing the printing temperature and layer thickness, it is possible to achieve the desired mechanical properties for 3D-printed parts, contributing to the development of more sustainable and environmentally friendly materials.

Moreover, thanks to the models created to predict the mechanical properties studied, 3D plots of the response surfaces of these properties are created in Figures A1–A6. These plots can approve the study of the feature importance.

#### 3.4.2. Analysis of the Response Surfaces

The response surfaces presented in Figures A1–A6 provide additional insights into the influence of the printing parameters on the mechanical properties of the PLA and PLA-CF specimens.

For PLA-CF, the response surfaces showed that the ultimate tensile strength decreases with increasing layer thickness and printing speed. The printing temperature had a more complex influence on the ultimate tensile strength, with the highest values observed in a range of temperatures between 210 °C and 225 °C. Young's modulus increased with increasing layer thickness at high printing speeds and low temperatures. The strain at break had its maximum values at a range of layer thicknesses between 0.375 mm and 0.425 mm, and increased with increasing printing temperature and decreasing printing speed.

For PLA, the response surfaces showed that printing temperature had the highest influence on the ultimate tensile strength, with an increase in strength observed with increasing temperature. Layer thickness had a significant influence on Young's modulus, with an increase in modulus observed with increasing layer thickness. The increase in printing speed also produced a higher Young's modulus. The maximum values of strain at break for PLA specimens appeared at a range of layer thicknesses between 0.375 mm and 0.425 mm, a range of printing speed between 45 mm/s and 55 mm/s, and at low temperatures.

These findings coincide with the studies of Othman et al. [8], who used PLA as the printing material, and layer thickness and other process parameters to study their influence on the mechanical properties of the printed parts, while Aissa et al. [12] used printing temperature, layer thickness, printing speed, and reinforced polyamide as the printing material. The findings also confirmed the importance of feature importance analysis, presented in the previous section, and the need for optimizing the printing parameters to achieve the desired mechanical properties.

### *3.5. Optimization of the Process Parameters*

After the analysis presented in Section 3.4, it is concluded that the material used had the most significant influence on the mechanical properties studied. Once the appropriate material is selected, the choice of the process parameters depends on the desired mechanical properties. Therefore, to optimize these relationships and find the optimal set of printing parameters for a given material, a genetic algorithm was used.

#### 3.5.1. Genetic Algorithm

The genetic algorithm (GA) is a population-based stochastic optimization algorithm that was inspired by Charles Darwin's theory of evolution. The GA algorithm begins by creating an initial population of multiple solutions that represent the chromosomes of the individuals. The fitness of each individual in the population is then evaluated by calculating a fitness score [33]. Natural selection is applied by selecting the fittest individuals from the population. Crossover and mutation are then applied to produce offspring that descend from the fittest individuals.

The crossover operator takes two parents and produces two offspring by exchanging parts of their chromosomes. The mutation operator introduces small random changes to the offspring's chromosomes to promote diversity in the population. These operators are

used to produce a new population, and the process of selection, crossover, and mutation is repeated until the termination criteria are achieved.

The use of GAs in 3D printing optimization has become increasingly popular in recent years due to its ability to efficiently find the optimal set of printing parameters. By using GAs, it is possible to search through a large parameter space and find the best set of parameters that result in the desired mechanical properties of the printed parts.

Figure 7 summarizes the GA process, showing the steps involved in generating the initial population, evaluating fitness, selecting the fittest individuals, and applying crossover and mutation to produce offspring for the next generation.

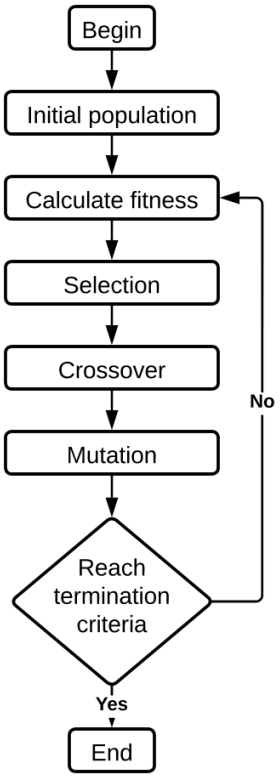


**Figure 7.** Flow chart of the genetic algorithm.

**Figure 7.** Flow chart of the genetic algorithm.

### 3.5.2. Optimization of the Process Parameters

3.5.2. Optimization of the Process Parameters

The fitness function used in the genetic algorithm plays a crucial role in determining the optimal set of process parameters. This study defines the fitness function as a weighted sum of the predicted mechanical properties using the process parameters. The weights of each mechanical property are determined by the user based on the application of the printed part and the importance of each property in the design criteria.

The fitness function used in the genetic algorithm plays a crucial role in determining the optimal set of process parameters. This study defines the fitness function as a weighted sum of the predicted mechanical properties using the process parameters. The weights of each mechanical property are determined by the user based on the application of the printed part and the importance of each property in the design criteria.

The fitness function (Equation (13)) includes the ultimate tensile strength, Young's modulus, and strain at break, as the predicted mechanical properties. The process parameters to optimize are the material ($m$) used, printing temperature ($t$), layer thickness ($h$), and printing speed ($s$). The predicted mechanical properties, $\hat{\sigma}$, $\hat{E}$, and $\hat{\epsilon}$, are calculated using the ensemble learning models trained in Section 3.3:

The fitness function (Equation (13)) includes the ultimate tensile strength, Young's modulus, and strain at break, as the predicted mechanical properties. The process parameters to optimize are the material ($m$) used, printing temperature ($t$), layer thickness ($h$), and printing speed ($s$). The predicted mechanical properties, $\hat{\sigma}$, $\hat{E}$, and $\hat{\epsilon}$, are calculated using the ensemble learning models trained in Section 3.3:

$$f(m,t,h,s) = \alpha \times \frac{\hat{\sigma}}{\bar{\sigma}} + \frac{\beta \times \hat{E}}{\bar{E}} + \frac{\gamma \times \hat{\epsilon}}{\bar{\epsilon}}. \quad (13)$$

$$f(m,t,h,s) = \alpha \times \frac{\hat{\sigma}}{\bar{\sigma}} + \frac{\beta \times \hat{E}}{\bar{E}} + \frac{\gamma \times \hat{\epsilon}}{\bar{\epsilon}}. \quad (13)$$

To normalize the mechanical properties, the average values of the mechanical properties in the collected data, $\bar{\sigma}$, $\bar{E}$, and $\bar{\epsilon}$, are used in the fitness function. This normalization is important to ensure that the optimization process is not biased toward a specific mechanical property. The weights of the mechanical properties, $\alpha$, $\beta$, and $\gamma$, are assigned by the user. These weights determine the importance of each mechanical property in the optimization process. The user can assign higher weights to the properties that are more critical to the application of the printed part.

To normalize the mechanical properties, the average values of the mechanical properties in the collected data, $\bar{\sigma}$, $\bar{E}$, and $\bar{\epsilon}$, are used in the fitness function. This normalization is important to ensure that the optimization process is not biased toward a specific mechanical property. The weights of the mechanical properties, $\alpha$, $\beta$, and $\gamma$, are assigned by the user.

By using the fitness function in the genetic algorithm, it is possible to efficiently search for the optimal set of process parameters that result in the desired mechanical

These weights determine the importance of each mechanical property in the optimization process. The user can assign higher weights to the properties that are more critical to the application of the printed part.

By using the fitness function in the genetic algorithm, it is possible to efficiently search for the optimal set of process parameters that result in the desired mechanical properties of the printed parts. This approach can significantly reduce the time and cost required to find the optimal printing parameters for a given material and application.



Equation (14) represents the range of values for the parameters that will be optimized by the genetic algorithm. The optimization process aims to maximize the fitness function while keeping the printing temperature, layer thickness, printing speed, and printing material within the specified range. By setting these boundaries, the GA algorithm can efficiently search for the optimal set of parameters that result in the desired mechanical properties of the printed parts. The range of values for each parameter is based on the experimental results obtained in the previous sections and represents the feasible and optimal values for the printing parameters.

$$\begin{cases} \text{maximize} f \\ m \in \{0,1\}; 0 \text{attributed to PLA and 1 attributed to PLA} - \text{CF} \\ 200\,^{\circ}\text{C} < t < 230\,^{\circ}\text{C} \\ 0.25 \text{ mm} < h < 0.45 \text{ mm} \\ 40 \text{ mm/s} < \text{s} < 60 \text{ mm/s} \end{cases} \quad (14)$$

During each generation, the fitness score of each individual is calculated using the weighted sum of predicted mechanical properties based on the parameters assigned by the user. The top five fittest individuals are then selected to create the next generation through crossover and mutation. This process is repeated until the termination criteria, which is set to a maximum of 250 generations, is reached.

Figure 8 shows the evolution of fitness scores over the 250 generations. As can be seen, the fitness score improves significantly from the initial population to the later generations. This indicates that the genetic algorithm is effective in finding the optimal set of parameters that maximize the desired mechanical properties. The best individual found by the algorithm provides the optimal combination of printing parameters to achieve the desired mechanical properties for the printed parts.

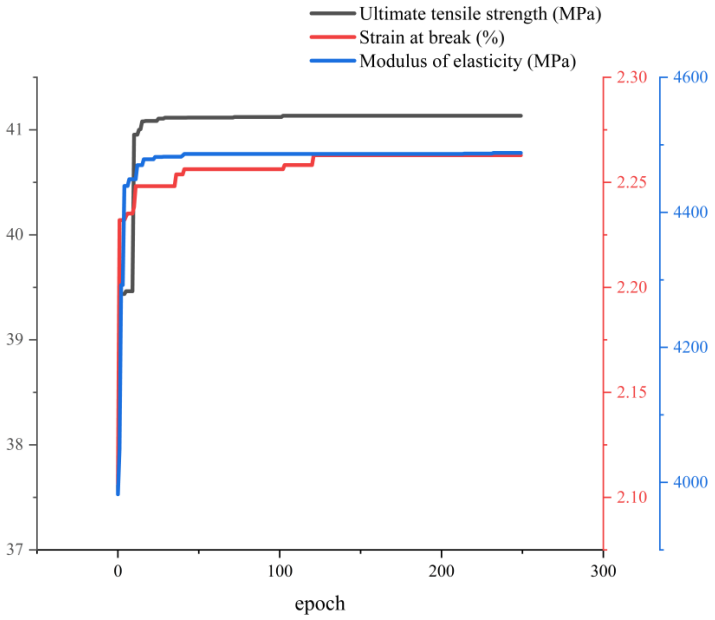


**Figure 8.** The optimal solution for each iteration of the optimization process for the mechanical properties.

**Figure 8.** The optimal solution for each iteration of the optimization process for the mechanical properties.

The results summarized in Table 6 show the optimal solutions for different mechanical properties using fused filament fabrication (FFF) 3D printing with PLA-CF (polylactic

The results summarized in Table 6 show the optimal solutions for different mechanical properties using fused filament fabrication (FFF) 3D printing with PLA-CF (polylactic acid—carbon fiber) and PLA (polylactic acid) materials. The optimal values and parameters for each property are as follows:

1. Ultimate tensile strength (UTS)—the optimum solution has a value of 41.129 MPa. The optimal parameters for achieving this value are:
   - Printing temperature: 222.28 °C;
   - Layer thickness: 0.261 mm;
   - Printing speed: 40.03 mm/s;
   - Material: PLA-CF.
2. Young's modulus—the optimal value is 4423.63 MPa, and the optimal parameters are:
   - Printing temperature: 200.01 °C;
   - Layer thickness: 0.388 mm;
   - Printing speed: 40.038 mm/s;
   - Material: PLA-CF.

**Table 6.** Solutions to the optimization process.

| Mechanical Property | Value | Material | Printing Temperature | Layer Thickness | Printing Speed |
|---|---|---|---|---|---|
| Ultimate tensile strength | 41.129 MPa | PLA-CF | 222.28 °C | 0.261 mm | 40.30 mm/s |
| Young's modulus | 4423.63 MPa | PLA-CF | 200.01 °C | 0.388 mm | 40.38 mm/s |
| Strain at break | 2.249% | PLA | 200.34 °C | 0.390 mm | 45.30 mm/s |

Note: In this case, the goal was to maximize Young's modulus, which is unusual. To search for the minimum, one could change the weight attributed to Young's modulus in the fitness function by changing its value to −1, for example.

3. Strain at break—the optimal solution has a value of 2.249%. The parameters for achieving this value are:
   - Printing temperature: 200.34 °C;
   - Layer thickness: 0.39 mm;
   - Printing speed: 45.30 mm/s;
   - Material: PLA.

According to the literature, as the layer thickness increases, the ultimate tensile strength decreases [33,34], which explains the low layer thickness value produced by the GA method. Furthermore, Huynh et al. [35] demonstrated that increasing the temperature from 200 °C to 220 °C, using PLA as a printing material, greatly enhances the ultimate tensile strength, which explains the printing temperature of 222.28 °C coming from the ultimate tensile strength optimization.

These results are confirmed by the response surfaces presented in Figures A1–A6. These figures demonstrate the relationships between the process parameters and the mechanical properties of the printed materials.

## 4. Conclusions and Prospects

This article presents a data-driven modeling approach to predict the ultimate tensile strength (UTS), Young's modulus, and strain at break of PLA and PLA-CF dog-bone specimens. The specimens were manufactured according to ASTM D638-14 Type I and tested using a universal tensile material testing system (MTS). The study investigated the influence of material type and process parameters such as printing temperature, printing speed, and layer thickness on the mechanical properties. A genetic algorithm was employed to optimize the process parameters for specific conditions. Ensemble learning algorithms, including XGBoost, gradient boosting regressor, random forest, decision tree, multiple linear regression, lasso, and ridge regression, were used to predict the mechanical properties with high accuracy.

This study has shown that PLA-CF specimens exhibit higher ultimate tensile strength (UTS) and Young's modulus compared to PLA specimens. For PLA-CF specimens, the following trends were observed in relation to process parameters:

- UTS increases when layer thickness and printing speed decrease, with maximum values at printing temperatures between 210 °C and 225 °C;
- Young's modulus increases with increasing layer thickness and printing speed and decreasing printing temperature;
- Strain at break increases with increasing printing temperature and decreasing printing speed, with maximum values for layer thicknesses between 0.375 mm and 0.425 mm.

For PLA specimens, the following trends were observed:

- Both UTS and Young's modulus increase when all studied process parameters (printing temperature, printing speed, and layer thickness) increase;
- Strain at break increases when printing temperature decreases, with maximum values for layer thicknesses between 0.375 mm and 0.425 mm, and printing speeds between 45 mm/s and 55 mm/s.

The genetic algorithm used in the study produced values of 41.129 MPa for UTS, 4423.63 MPa for Young's modulus, and 2.249% for strain at break.

The study focused on the effect of printing materials (PLA and PLA-CF) and process parameters (printing speed, printing temperature, and layer thickness) on the mechanical properties of 3D printed parts. Future research aims to investigate the influence of additional process parameters, such as infill density and bed temperature, on the mechanical properties of 3D-printed parts, as well as to explore more materials to broaden the scope of the study.

**Author Contributions:** Conceptualization, A.Z.; formal analysis, M.H. and A.Z.; funding acquisition, M.H. and S.K.; investigation, A.Z.; methodology, M.H.; software, A.Z.; supervision, M.H. and S.K.; writing—original draft, A.Z.; writing—review and editing, M.H. All authors have read and agreed to the published version of the manuscript.

**Funding:** The authors acknowledge the funding provided by the Natural Sciences and Engineering Research Council (NSERC) of Canada (grant number: CRSNG–RGPIN-2021-02846) and the Canada Research Chair Program.

**Data Availability Statement:** Data available under request.

**Conflicts of Interest:** The authors certify that they have no affiliations with or involvement in any organization or entity with any financial interest or non-financial interest in the subject matter or materials discussed in this manuscript.

## Appendix A

**Table A1.** The preprocessed collected data from the mechanical test.

| PLA Run | Ultimate Tensile Strength ($\sigma$) | Modulus of Elasticity (E) | Strain at Break ($\epsilon$) | PLA-CF Run | Ultimate Tensile Strength ($\sigma$) | Young's Modulus (E) | Strain at Break ($\epsilon$) |
|---|---|---|---|---|---|---|---|
| 1 | 26.66 | 1746.67 | 1.79 | 1 | 33.61 | 3754.25 | 1.42 |
| 2 | 25.92 | 1744.65 | 1.84 | 2 | 34.17 | 3356.07 | 1.44 |
| 3 | 27.34 | 1505.78 | 2.00 | 3 | 34.44 | 3497.39 | 1.55 |
| 4 | 24.50 | 1543.07 | 1.95 | 4 | 37.93 | 4391.66 | 1.16 |
| 5 | 26.85 | 1202.43 | 2.31 | 5 | 38.14 | 4174.61 | 1.30 |
| 6 | 25.93 | 1482.00 | 1.96 | 6 | 37.61 | 4581.69 | 1.10 |
| 7 | 31.41 | 1812.83 | 2.08 | 7 | 35.85 | 4125.07 | 1.08 |
| 8 | 29.42 | 1891.01 | 1.89 | 8 | 35.74 | 4132.72 | 1.10 |
| 9 | 24.30 | 1258.48 | 2.18 | 9 | 31.13 | 3984.64 | 0.92 |
| 10 | 27.23 | 1556.10 | 1.96 | 10 | 39.60 | 3505.53 | 1.56 |

**Table A1.** *Cont.*

| PLA Run | Ultimate Tensile Strength ($\sigma$) | Modulus of Elasticity (E) | Strain at Break ($\epsilon$) | PLA-CF Run | Ultimate Tensile Strength ($\sigma$) | Young's Modulus (E) | Strain at Break ($\epsilon$) |
|---|---|---|---|---|---|---|---|
| 11 | 30.20 | 2143.89 | 1.97 | 11 | 37.34 | 3986.06 | 1.30 |
| 12 | 31.21 | 1629.61 | 2.06 | 12 | 37.39 | 3853.34 | 1.38 |
| 13 | 28.87 | 1809.15 | 1.92 | 13 | 38.53 | 4153.85 | 1.44 |
| 14 | 28.39 | 1762.37 | 1.94 | 14 | 36.99 | 4000.50 | 1.30 |
| 15 | 27.16 | 1617.90 | 2.024 | 15 | 36.31 | 4060.63 | 1.22 |
| 16 | 33.59 | 1801.88 | 2.15 | 16 | 35.57 | 3768.16 | 1.37 |
| 17 | 29.87 | 1756.94 | 1.83 | 17 | 35.88 | 3939.81 | 1.22 |
| 18 | 25.90 | 1625.23 | 1.717 | 18 | 34.43 | 4034.85 | 1.06 |
| 19 | 30.21 | 1895.71 | 2.054 | 19 | 31.40 | 3497.64 | 1.37 |
| 20 | 32.03 | 1755.01 | 2.39 | 20 | 34.65 | 4250.31 | 1.38 |
| 21 | 32.95 | 2094.29 | 1.90 | 21 | 34.88 | 3941.19 | 1.51 |
| 22 | 30.64 | 1958.45 | 1.82 | 22 | 35.05 | 3339.23 | 1.70 |
| 23 | 30.38 | 1881.98 | 1.80 | 23 | 34.24 | 3518.94 | 1.47 |
| 24 | 29.65 | 1922.06 | 1.79 | 24 | 34.53 | 3256.32 | 1.79 |
| 25 | 26.15 | 1897.19 | 1.45 | 25 | 32.76 | 3343.46 | 1.37 |
| 26 | 29.91 | 1931.47 | 1.85 | 26 | 33.24 | 3432.23 | 1.33 |
| 27 | 31.54 | 2011.35 | 1.85 | 27 | 34.89 | 3912.19 | 1.22 |



## Appendix B

Appendix B

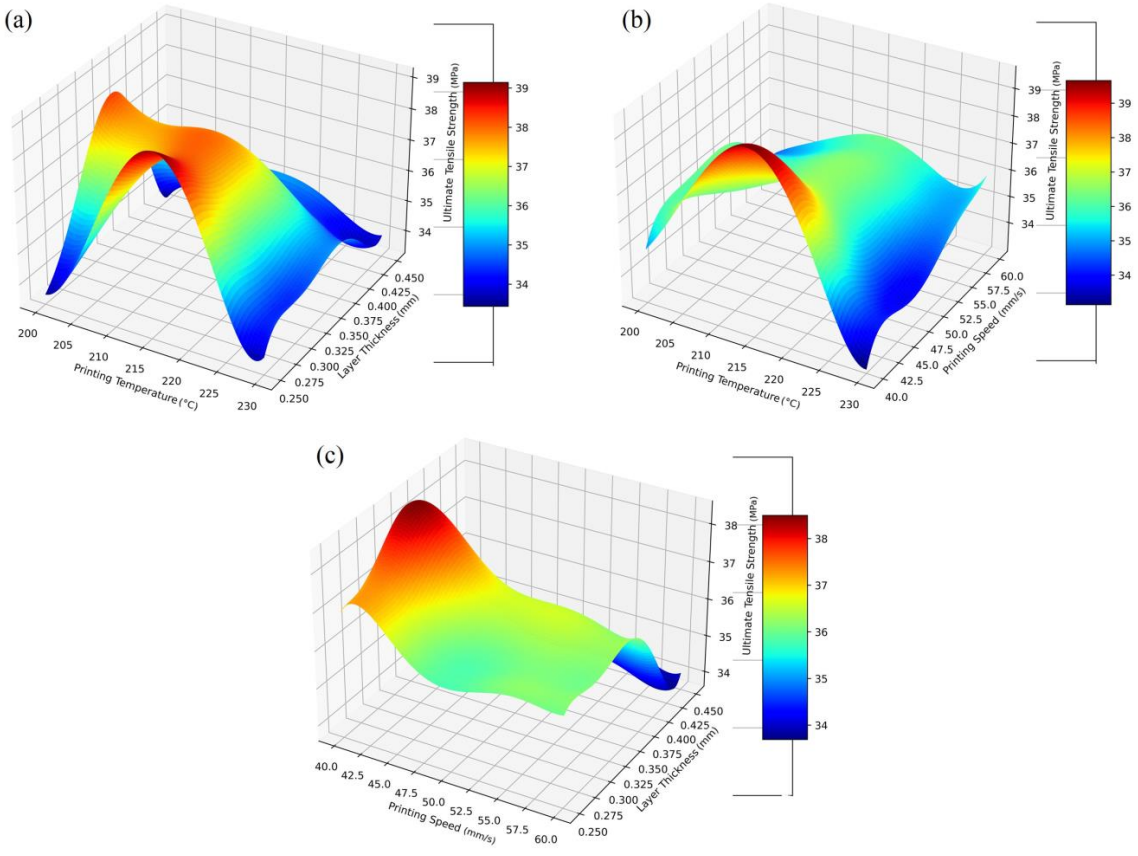


**Figure A1.** Response surface 3D plots of the predicted ultimate tensile strength of PLA-CF: (**a**) printing temperature vs. layer thickness, (**b**) printing temperature vs. printing speed, and (**c**) printing speed vs. layer thickness.

**Figure A1.** Response surface 3D plots of the predicted ultimate tensile strength of PLA-CF: (**a**) printing temperature vs. layer thickness, (**b**) printing temperature vs. printing speed, and (**c**) printing speed vs. layer thickness.

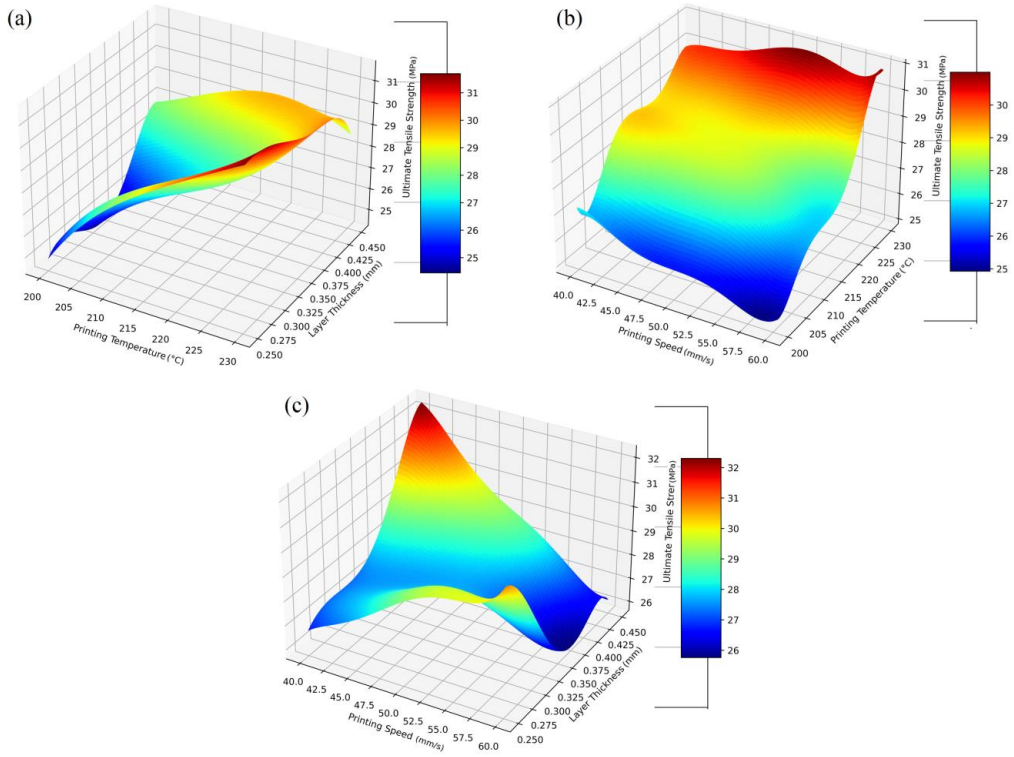


**Figure A2.** Response surface 3D plots of the predicted ultimate tensile strength of PLA: (**a**) printing temperature vs. layer thickness, (**b**) printing speed vs. printing temperature, and (**c**) printing speed vs. layer thickness.

*Eng* **2023**, *4*, FOR PEER REVIEW 23

**Figure A2.** Response surface 3D plots of the predicted ultimate tensile strength of PLA: (**a**) printing temperature vs. layer thickness, (**b**) printing speed vs. printing temperature, and (**c**) printing speed vs. layer thickness.

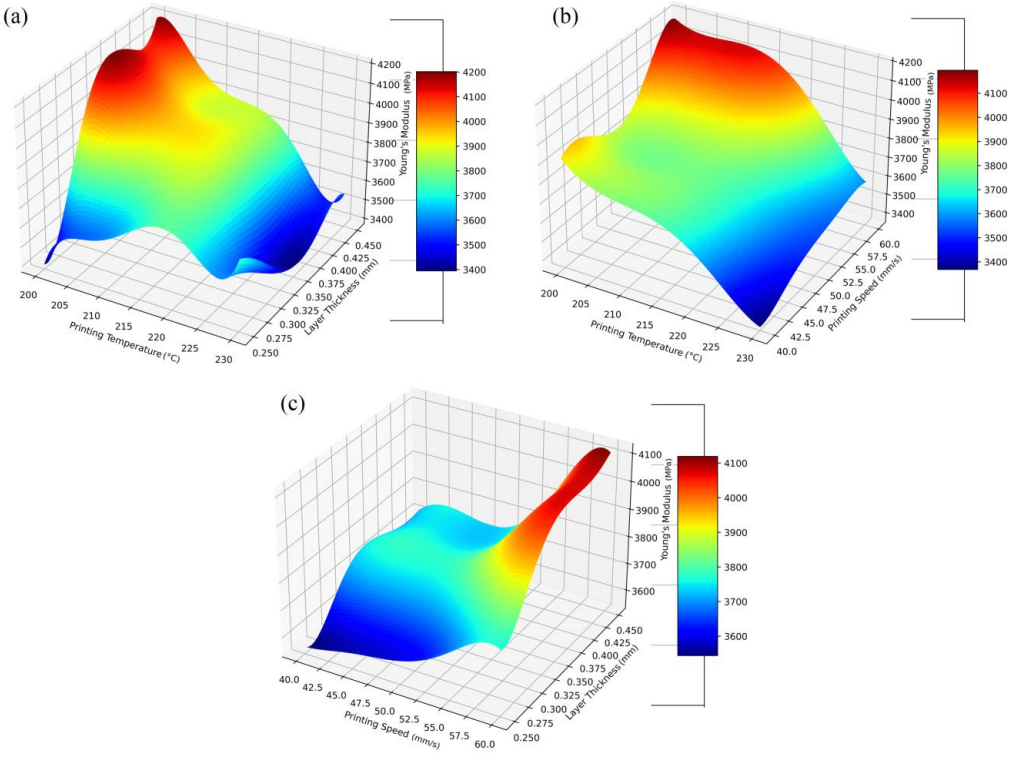


**Figure A3.** Response surface 3D plots of the predicted Young's modulus of PLA-CF: (**a**) printing temperature vs. layer thickness, (**b**) printing temperature vs. printing speed, and (**c**) printing speed vs. layer thickness.

**Figure A3.** Response surface 3D plots of the predicted Young's modulus of PLA-CF: (**a**) printing temperature vs. layer thickness, (**b**) printing temperature vs. printing speed, and (**c**) printing speed vs. layer thickness.

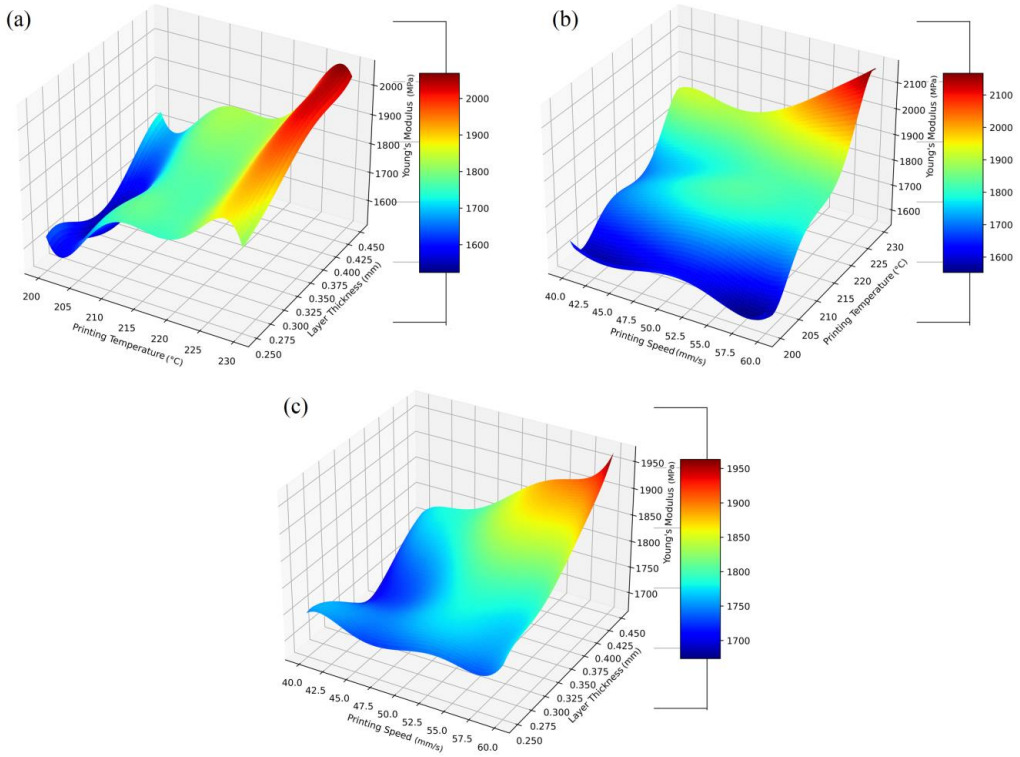


**Figure A4.** Response surface 3D plots of the predicted Young's modulus of PLA: (**a**) printing temperature vs. layer thickness, (**b**) printing speed vs. printing temperature, and (**c**) printing speed vs. layer thickness.

*Eng* **2023**, *4*, FOR PEER REVIEW 25

**Figure A4.** Response surface 3D plots of the predicted Young's modulus of PLA: (**a**) printing temperature vs. layer thickness, (**b**) printing speed vs. printing temperature, and (**c**) printing speed vs. layer thickness.

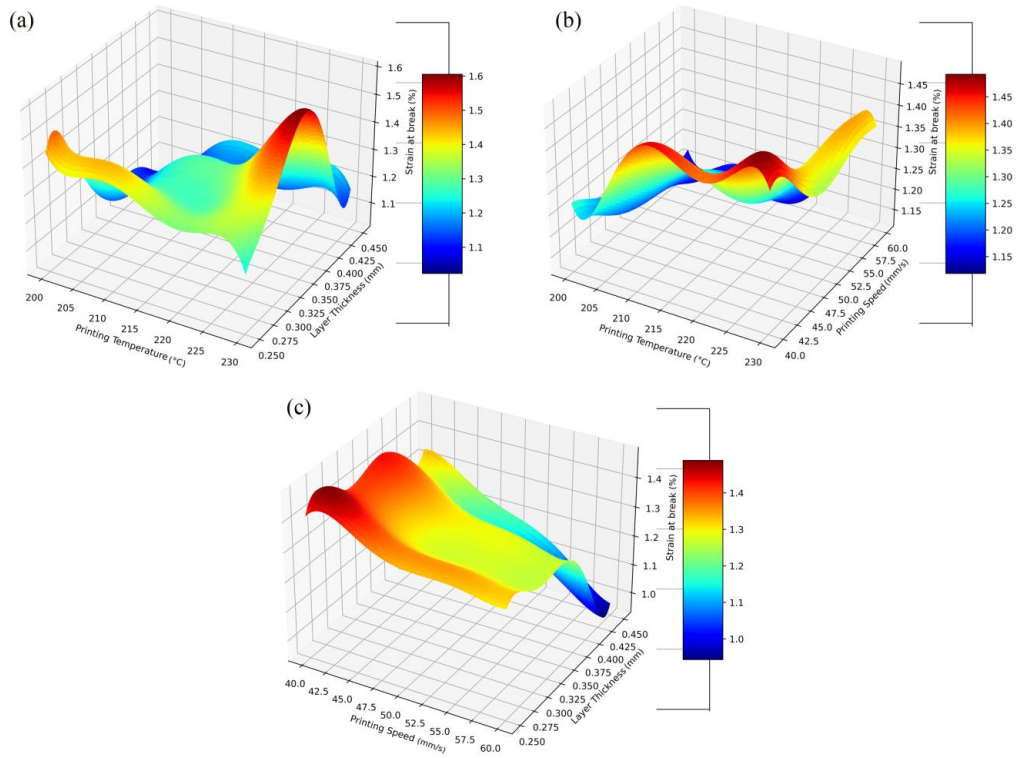


**Figure A5.** Response surface 3D plots of the predicted strain at break of PLA-CF: (**a**) printing temperature vs. layer thickness, (**b**) printing temperature vs. printing speed, and (**c**) printing speed vs. layer thickness.

**Figure A5.** Response surface 3D plots of the predicted strain at break of PLA-CF: (**a**) printing temperature vs. layer thickness, (**b**) printing temperature vs. printing speed, and (**c**) printing speed vs. layer thickness.

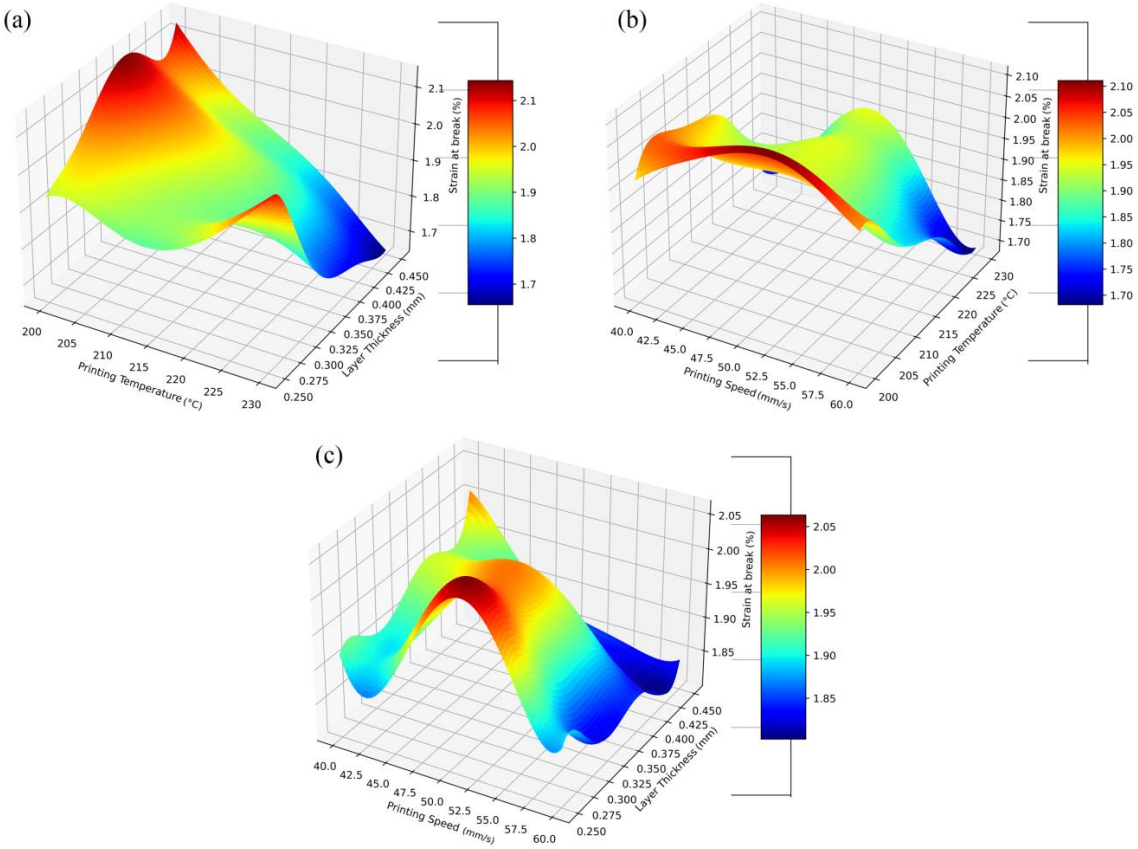


**Figure A6.** Response surface 3D plots of the predicted strain at break of PLA: (**a**) printing temperature vs. layer thickness, (**b**) printing speed vs. printing temperature, and (**c**) printing speed vs. layer thickness.

**Figure A6.** Response surface 3D plots of the predicted strain at break of PLA: (**a**) printing temperature vs. layer thickness, (**b**) printing speed vs. printing temperature, and (**c**) printing speed vs. layer thickness.

## References

1. Khosravani, M.R.; Reinicke, T. On the environmental impacts of 3D printing technology. *Appl. Mater. Today* **2020**, *20*, 100689. [CrossRef]
2. Shaqour, B.; Abuabiah, M.; Abdel-Fattah, S.; Juaidi, A.; Abdallah, R.; Abuzaina, W.; Qarout, M.; Verleije, B.; Dos, P. Gaining a better understanding of the extrusion process in fused filament fabrication 3D printing: A review. *Int. J. Adv. Manuf. Technol.* **2021**, *114*, 1279–1291. [CrossRef]
3. Radadiya, V.A.; Gandhi, A.H. A Study of Tensile Characteristics for Glass and Carbon Fiber Along with Sandwiched Reinforced ABS Composites. *J. Inst. Eng. (India) Ser. C* **2022**, *103*, 1049–1057. [CrossRef]
4. Farhan Khan, M.; Alam, A.; Ateeb Siddiqui, M.; Saad Alam, M.; Rafat, Y.; Salik, N.; Al-Saidan, I. Real-time defect detection in 3D printing using machine learning. *Mater. Today Proc.* **2020**, *42*, 521–528. [CrossRef]
5. Gebisa, A.W.; Lemu, H.G. Influence of 3D printing FDM process parameters on tensile property of ultem 9085. *Procedia Manuf.* **2019**, *30*, 331–338. [CrossRef]
6. Rodríguez-Panes, A.; Claver, J.; Camacho, A.M. The influence of manufacturing parameters on the mechanical behaviour of PLA and ABS pieces manufactured by FDM: A comparative analysis. *Materials* **2018**, *11*, 1333. [CrossRef]
7. Chokshi, H.; Shah, D.B.; Patel, K.M.; Joshi, S.J. Experimental investigations of process parameters on mechanical properties for PLA during processing in FDM. *Adv. Mater. Process. Technol.* **2022**, *8* (Suppl. 2), 696–709. [CrossRef]
8. Othman, F.M.; Fadhil, T.; Ali, A.H.B. Influence of process parameters on mechanical properties and printing time of FDM PLA printed parts using design of experiment. *J. Eng. Res.* **2018**, *8*, 2248–9622.
9. Ning, F.; Cong, W.; Qiu, J.; Wei, J.; Wang, S. Additive manufacturing of carbon fiber reinforced thermoplastic composites using fused deposition modeling. *Compos. Part B Eng.* **2015**, *80*, 369–378. [CrossRef]
10. Love, L.J.; Kunc, V.; Rios, O.; Duty, C.E.; Elliott, A.M.; Post, B.K.; Smith, R.J.; Blue, C.A. The importance of carbon fiber to polymer additive manufacturing. *J. Mater. Res.* **2014**, *29*, 1893–1898. [CrossRef]
11. Torrado Perez, A.R.; Roberson, D.A.; Wicker, R.B. Fracture surface analysis of 3D-printed tensile specimens of novel ABS-based materials. *J. Fail. Anal. Prev.* **2014**, *14*, 343–353. [CrossRef]
12. Ouballouch, A.; Alaiji, R.E.; Ettaqi, S.; Bouayad, A.; Sallaou, M.; Lasri, L. Evaluation of dimensional accuracy and mechanical behavior of 3D printed reinforced polyamide parts. *Procedia Struct. Integr.* **2019**, *19*, 433–441. [CrossRef]

13. Mushtaq, R.T.; Iqbal, A.; Wang, Y.; Rehman, M.; Petra, M.I. Investigation and Optimization of Effects of 3D Printer Process Parameters on Performance Parameters. *Materials* **2023**, *16*, 3392. [CrossRef] [PubMed]
14. Zhang, Z.; Shi, J.; Yu, T.; Santomauro, A.; Gordon, A.; Gou, J.; Wu, D. Predicting flexural strength of additively manufactured continuous carbon fiber- reinforced polymer composites using machine learning. *J. Comput. Inf. Sci. Eng.* **2020**, *20*, 061015. [CrossRef]
15. Goh, G.D.; Yap, Y.L.; Tan, H.K.; Sing, S.L.; Goh, G.L.; Yeong, W.Y. Process-structure-properties in polymer additive manufacturing via material extrusion: A review. *Crit. Rev. Solid State Mater. Sci.* **2020**, *45*, 113–133. [CrossRef]
16. Maulud, D.; Abdulazeez, A.M. A Review on Linear Regression Compre- hensive in Machine Learning. *J. Appl. Sci. Technol. Trends* **2020**, *1*, 140–147. [CrossRef]
17. Huang, J.H.R.; Wu, C.-Y.; Chan, H.-M.; Ciou, J.-Y. Printing parameters of Sugar/Pectin Jelly Candy and application by using a decision tree in a hot-extrusion 3D printing system. *Sustainability* **2022**, *14*, 11618. [CrossRef]
18. Barrios, J.M.; Romero, P.E. Decision tree methods for predicting surface roughness in fused deposition modeling parts. *Materials* **2019**, *12*, 2574. [CrossRef]
19. Ghojogh, B.; Crowley, M. The theory behind overfitting, cross validation, regularization, bagging, and boosting: Tutorial. *arXiv* **2019**, arXiv:1905.12787. [CrossRef]
20. Ma, Y.; Schutyser, M.A.; Boom, R.M.; Zhang, L. Predicting the extrudability of complex food materials during 3D printing based on image analysis and gray-box data-driven modelling. *Innov. Food Sci. Emerg. Technol.* **2021**, *73*, 102764. [CrossRef]
21. Li, X.; Zhang, M.; Zhou, M.; Wang, J.; Zhu, W.; Wu, C.; Zhang, X. Qualify assessment for extrusion-based additive manufacturing with 3D scan and machine learning. *J. Manuf. Process.* **2023**, *90*, 274–285. [CrossRef]
22. Lee, S.; Park, J.; Kim, N.; Lee, T.; Quagliato, L. Extreme Gradient Boosting-inspired process optimization algorithm for manufacturing engineering applications. *Mater. Des.* **2023**, *226*, 111625. [CrossRef]
23. Cai, R.; Wang, K.; Wen, W.; Peng, Y.; Baniassadi, M.; Ahzi, S. Application of machine learning methods on dynamic strength analysis for additive manufactured polypropylene-based composites. *Polym. Test.* **2022**, *110*, 107580. [CrossRef]
24. Wu, T.; Zhang, W.; Jiao, X.; Guo, W.; Alhaj Hamoud, Y. Evaluation of stacking and blending ensemble learning methods for estimating daily reference evapotranspiration. *Comput. Electron. Agric.* **2021**, *184*, 106039. [CrossRef]
25. Cui, S.; Yin, Y.; Wang, D.; Li, Z.; Wang, Y. A stacking-based ensemble learning method for earthquake casualty prediction. *Appl. Soft Comput.* **2021**, *101*, 107038. [CrossRef]
26. Sun, W.; Trevor, B. A stacking ensemble learning framework for annual river ice breakup dates. *J. Hydrol.* **2018**, *561*, 636–650. [CrossRef]
27. Gupta, A.K.; Taufik, M. Investigation of dimensional accuracy of material extrusion build parts using mathematical modelling and artificial neural network. *Int. J. Interact. Des. Manuf.* **2023**, *17*, 869–885. [CrossRef]
28. Chicco, D.; Warrens, M.J.; Jurman, G. The coefficient of determination R-squared is more informative than SMAPE, MAE, MAPE, MSE and RMSE in regression analysis evaluation. *PeerJ Comput. Sci.* **2021**, *7*, e623. [CrossRef]
29. Materials, P.; Materials, E.I. *Standard Test Method for Tensile Properties of Plastics*; ASTM: West Conshohocken, PA, USA, 2015; Volume 1, pp. 1–17.
30. Butt, J.; Bhaskar, R.; Mohaghegh, V. Investigating the effects of extrusion temperatures and material extrusion rates on FFF-printed thermoplastics. *Int. J. Adv. Manuf. Technol.* **2021**, *117*, 2679–2699. [CrossRef]
31. Wang, P.; Zou, B.; Xiao, H.; Ding, S.; Huang, C. Effects of printing parameters of fused deposition modeling on mechanical properties, surface quality, and microstructure of PEEK. *J. Mater. Process. Technol.* **2019**, *271*, 62–74. [CrossRef]
32. Spoerk, M.; Holzer, C.; Gonzalez-Gutierrez, J. Material extrusion-based additive manufacturing of polypropylene: A review on how to improve dimensional inaccuracy and warpage. *J. Appl. Polym. Sci.* **2020**, *137*, 48545. [CrossRef]
33. Feng, R.; Jiang, J.; Sun, Z.; Thakur, A.; Wei, X. A hybrid of genetic algorithm and particle swarm optimization for reducing material waste in extrusion-based additive manufacturing. *Rapid Prototyp. J.* **2021**, *27*, 1872–1885. [CrossRef]
34. Srinivasan, R.; Prathap, P.; Raj, A.; Kannan, S.A.; Deepak, V. Influence of fused deposition modeling process parameters on the mechanical properties of PETG parts. *Mater. Today Proc.* **2020**, *27*, 1877–1883. [CrossRef]
35. Huynh, L.P.T.; Nguyen, H.A.; Phan, L.K.H.; Tran, T.T. Effect of process parameters on mechanical strength of fabricated parts using the fused deposition modelling method. *J. Korean Soc. Precis. Eng.* **2019**, *36*, 705–712. [CrossRef]